https://doi.org/10.5194/egusphere-2026-6609
Preprint. Discussion started: 4 November 2026
© Author(s) 2026. CC BY 4.0 License.

Contrasting 3-D Structures of Estonian Rapakivi Intrusions: Insights from Gravity and Magnetic Inversion Within the Paldiski–Pskov Deformation Zone

Juan David Solano-Acosta
Department of Geology, Tallinn University of Technology, Ehitajate tee 5, Tallinn, 19086, Estonia

Correspondence: Juan David Solano-Acosta (jusola@ttu.ee)

Abstract.

Estonia's Mesoproterozoic (∼1.6 Ga) Rapakivi intrusions are hosted within a structurally complex Precambrian basement influenced by the Paldiski-Pskov Deformation Zone (PPDZ) and are largely concealed beneath Phanerozoic sedimentary cover. Their subsurface geometries, depth extents, and structural relationships remain incompletely constrained. We investigated the Märjamaa-Kloostri, Naissaare, and Neeme intrusions to a model depth of ∼ 15 km using gravity and magnetic data, spectral filtering, potential-field derivatives, upward continuation, and three-dimensional joint inversion with SimPEG. Regional gravity and magnetic gradients broadly follow the NW-SE orientation of the PPDZ, whereas the recovered density-contrast and magnetic-susceptibility models reveal distinct subsurface architectures. Märjamaa exhibits a shallow concentric geometry consistent with piston-cauldron emplacement, underlain by heterogeneous, vertically organised geophysical domains extending below the depth investigated in previous local-scale models. Kloostri Phase III displays a comparatively tabular geometry adjacent to the northeastern margin of Märjamaa Phase II. Naissaare exhibits a vertically extensive magnetic structure partly offset from shallower, heterogeneous density domains, potentially reflecting deeper intrusive or magma-transfer components. Neeme produces weaker geophysical contrasts, combining a shallow density body with deeper, laterally displaced magnetic anomalies. The correspondence between recovered geophysical domains and mapped magmatic phases varies among the intrusions, highlighting differences in their internal petrophysical architecture. Although their regional setting is associated with the PPDZ, the inversion does not resolve continuous subsurface connections between the three intrusive systems. These findings suggest that the Estonian Rapakivi intrusions developed within a shared tectonomagmatic framework while preserving distinct subsurface geometries and physical-property distributions, potentially reflecting differences in magma emplacement, structural accommodation, and local crustal conditions.

1 Introduction

Rapakivi granites are a distinctive group of ferroan A-type granitoids that occur widely in Proterozoic terranes and are especially abundant across the Fennoscandian Shield (Haapala and Rämö, 1992; Rämö and Haapala, 1995, 2005; Vigneresse, 2005; Salminen et al., 2021). They commonly form part of bimodal anorthosite-mangerite-charnockite-granite (AMCG) associations

https://doi.org/10.5194/egusphere-2026-6609
Preprint. Discussion started: 4 November 2026
© Author(s) 2026. CC BY 4.0 License.

and are generally associated with post-orogenic to intraplate magmatism (Emslie, 1978; Loiselle and Wones, 1979; Bonin, 2007; Dall'Agnol et al., 2005; Sharkov, 2010; Salminen et al., 2021; Johansson, 2023). In Fennoscandia, Rapakivi magmatism occurred mainly between ~ 1.67 and 1.44 Ga, during the Subjotnian interval, and formed several temporally distinct intrusive suites (Laitakari et al., 1996; Rämö et al., 1996; Puura and Flodén, 2000; Salminen et al., 2021; Grabarczyk et al., 2023). The oldest major episode, the Wiborg Suite (1.67-1.62 Ga), comprises the Wiborg batholith in southern Finland and the mainland Rapakivi granitoids of Estonia (Klein et al., 1994; Rämö et al., 1996; Puura and Flodén, 2000).

These Mesoproterozoic intrusions were emplaced within a Paleoproterozoic crustal architecture inherited from the Svecofennian orogeny (Fig.1a) (Kukkonen and Lauri, 2009; Nordbäck et al., 2024; Solano-Acosta et al., 2025a; Lahtinen and Kurhila, 2026). Regional geophysical and structural studies show that the Fennoscandian crust contains long-lived discontinuities, shear zones, and fault-bounded domains that locally influenced magma transport and emplacement (Korja et al., 1993; Elo and Korja, 1993; BABEL Working Group, 1993a, b; Korja and Heikkinen, 1995; Puura and Flodén, 2000; Bogdanova et al., 2015). In western and northern Estonia, the Paldiski-Pskov Deformation Zone (PPDZ) is one such major crustal structure and provides an important regional framework for understanding the distribution and emplacement of several Rapakivi bodies (Puura and Flodén, 1999, 2000; Solano Acosta, 2026).

In Estonia, Rapakivi granitoids are largely concealed beneath Palaeozoic sedimentary cover. They include Naissaare, Märjamaa, Kloostri, Neeme, Taebla, and Ereda, as well as the larger Riga batholith (Soesoo and Niin, 1992; Klein et al., 1994; Rämö et al., 1996; Laitakari et al., 1996; Kirs et al., 2004) (Fig.1b). These bodies are mainly syeno- to monzogranitic and commonly have porphyritic textures with microcline megacrysts, although the classic plagioclase-mantled Rapakivi texture is not present in all of them (Soesoo and Niin, 1992; Soesoo, 1993; Klein et al., 1994; Raukas and Teedumäe, 1997). Although relatively small in mapped area compared with the main Finnish Wiborg batholith, their geochemical and isotopic characteristics support their classification as part of the broader Fennoscandian Rapakivi system (Soesoo and Niin, 1992; Klein et al., 1994; Rämö et al., 1996; Potagin, 2024; Solano-Acosta et al., 2026c). Because basement exposures are limited, the mapped outlines of these bodies provide only partial constraints on their true lateral extent, internal architecture, and continuation at depth.

https://doi.org/10.5194/egusphere-2026-6609
Preprint. Discussion started: 4 November 2026
© Author(s) 2026. CC BY 4.0 License.

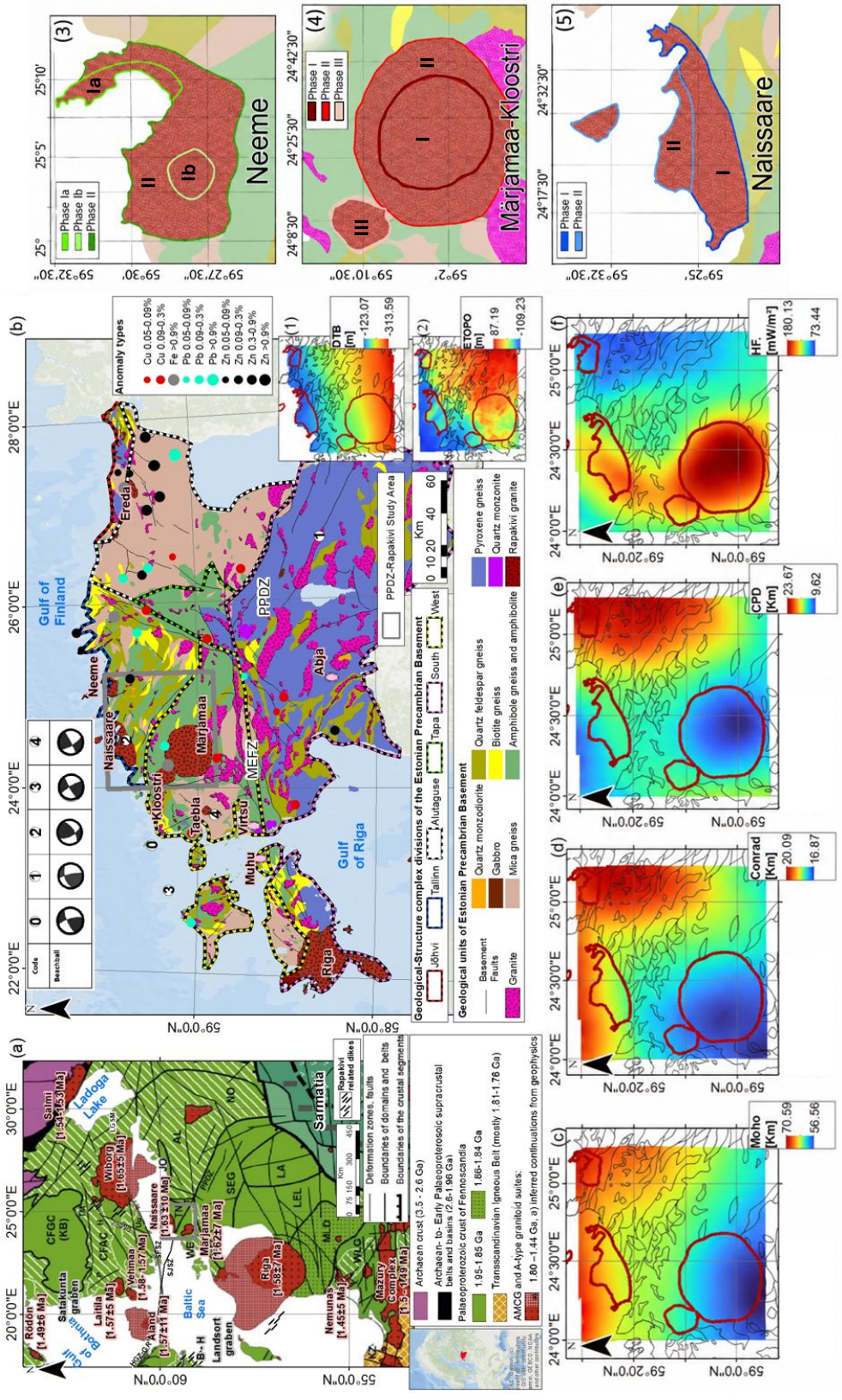


Figure 1. Geological setting of the study zone. (**a**) Major Paleoproterozoic tectonic domains of Fennoscandia, modified after Bogdanova et al. (2015), highlighting the most prominent Rapakivi bodies, with the Märjamaa and Kloostri granitoids study area marked by a red rectangle. The white diagonal ruling over the greenish area indicates Svecofennian sedimentary basins. The abbreviations are AL – Alutaguse, B-H - Breven-Hällefors dike swarms, CFAS – Central Finland Arc Complex, CFGC – Central Finland Granitoid Complex, H – Häme belt, HGZ-GR – Hagsta-Gävle-Rättvik Zone, JO – Jõhvi, KB – Keitele microcontinent, LA – Latgalia, LEL – Latvian-East Lithuanian, MLD – Mid-Lithuanian domain, P – Pirkanmaa belt, SEG – South Estonian granulite domain, T – Tapa, TN – Tallinn, TM – Tampere belt, Uu – Uusimaa belt, WE – West Estonian domain, WLG – West Lithuanian granulite domain. Shear and fault zones are abbreviated as follows: MEFZ – Middle

https://doi.org/10.5194/egusphere-2026-6609
Preprint. Discussion started: 4 November 2026
© Author(s) 2026. CC BY 4.0 License.

Figure 1. *(continued)* Estonian Fault Zone, PMSZ – Porkkala–Mäntsälä Shear Zone, PPDZ – Paldiski-Pskov Deformation Zone, SFSZ – South Finland Shear Zone, and SJSZ – Sottunga-Jurmo Shear Zone. Age Rapakivi granitoids of Fennoscandia are constrained from Laitakari et al. (1996); Ahl (1997); Rämö et al. (1996); Skridlaitė et al. (2007); Larin (2009); Sharkov (2010); Johansson et al. (2016); Grabarczyk et al. (2023). **(b)** Precambrian geological map highlighting the Estonia basement, showing metalliferous anomalies based on Soesoo et al. (2020). The epicentres of the earthquakes analysed by Soosalu et al. (2022) are shown as white dots labelled with a number ("Code"), each with its respective focal mechanism (See Table 2 in Soosalu et al. (2022)), enhancing expressions of a predominantly left-lateral strike-slip movement on NW-SE to NNW-SSE subvertical faults. Geological data are available from the Land Board Geoportal of the Republic of Estonia (https://xgis.maaamet.ee/xgis2/page/app/geoloogia400k), including **(1)** Depth to Basement (DTB) measurements from the same source. **(2)** Elevation data is derived from ETOPO elevation model from the NOAA National Centers for Environmental Information. **(3-5)** The Neeme, Märjamaa-Kloostri, and Naissaare intrusions are zoomed and superimposed on the corresponding plutonic phases as defined by Klein et al. (1994). **(c - f)** Geophysical measurements from the studied zone updated from Solano-Acosta et al. (2023): **(c)** Moho discontinuity, **(d)** Conrad discontinuity, **(e)** Curie Point Depth (CPD), and **(f)** Heat flow.

Potential field methods are useful for investigating concealed Estonian Rapakivi intrusions. In southern Fennoscandia, gravity and magnetic data have been used to identify granitoid bodies and infer their subsurface geometry within the crystalline basement (Elo and Korja, 1993; Korja and Heikkinen, 1995; Puura and Flodén, 1996; All et al., 2004, 2006; Solano-Acosta et al., 2023, 2025a). Three-dimensional inversion provides better constraints on the vertical architecture and deeper continuity of these concealed systems by estimating their volumetric distributions and petrophysical properties (Solano-Acosta et al., 2025a; Solano Acosta, 2026). In Estonia, previous integrated modelling of the Märjamaa-Kloostri complex combined residual Bouguer gravity, magnetic data, structural interpretation, and 3-D SimPEG inversion to resolve the system to a depth of approximately 10 km, highlighting the role of the PPDZ in its emplacement (All et al., 2004; Solano-Acosta et al., 2025a). Petrographic and geochemical studies have independently documented the differentiation of its intrusive phases (Soesoo and Niin, 1992; Klein et al., 1994; Potagin, 2024; Solano-Acosta et al., 2026c; Solano-Acosta, 2026). Nevertheless, comparable three-dimensional geophysical constraints remain limited for other Estonian Rapakivi bodies, particularly across the larger PPDZ region.

This study builds on previous potential-field methods by examining a regional area encompassing the Märjamaa-Kloostri, Naissaare, and Neeme granitoids (Fig.1b). It uses Bouguer gravity and magnetic data, together with spectral filtering, upward continuation, key potential-field derivatives, and 3D SimPEG inversion, to investigate the subsurface structure of these concealed intrusions. The larger model domain provides a basis for comparing the shapes and physical properties of several Rapakivi bodies within the same regional context and analysing their spatial relationships with the PPDZ. The main goal is to develop a 3-D regional geophysical model of the granitoids and examine their subsurface geometries, densities, and magnetic susceptibilities. This will help define the extent and internal structure of the concealed Estonian Mesoproterozoic Rapakivi intrusions within the PPDZ framework. In this study, the PPDZ serves as a regional geological reference for the distribution of Rapakivi bodies, rather than as a target for detailed tectonic reconstruction.

https://doi.org/10.5194/egusphere-2026-6609
Preprint. Discussion started: 4 November 2026
© Author(s) 2026. CC BY 4.0 License.

2 Geological Setting

2.1 Regional context

The Estonian crystalline basement forms part of the Paleoproterozoic Fennoscandian crust and is dominated by metavolcanic, metasedimentary, and granitoid rocks formed and reworked during the Svecofennian orogeny (∼ 2.1-1.79 Ga) (Nironen, 1997; Lahtinen et al., 2005; Bogdanova et al., 2015; Soesoo et al., 2020). Following crustal stabilisation, Mesoproterozoic A-type magmatism produced the Fennoscandian Rapakivi-AMCG suites during the Subjotnian interval (∼ 1.67-1.45 Ga), several of which extend beneath sedimentary cover (BABEL Working Group, 1993a, b; Elo and Korja, 1993; Korja and Heikkinen, 1995; Laitakari et al., 1996; Puura and Flodén, 1996, 2000; All et al., 2006; Salminen et al., 2021; Solano-Acosta et al., 2023; Lahtinen and Kurhila, 2026). These intrusions are commonly grouped into four principal age intervals (Fig.1a): the Wiborg Suite (1.67-1.62 Ga), including Wiborg, Bodom, Obbnäs, Naissaare, Märjamaa, and Kloostri; the Åland Suite (1.59-1.56 Ga), including Ri Ga, Åland, Laitila, and Vehmaa; the Salmi Suite (1.55-1.53 Ga) near the Archean-Proterozoic boundary; and the Ragunda Suite (1.53-1.47 Ga), including Ragunda and Rödon Swedish plutons and the Mazury complex (Suominen, 1991; Klein et al., 1994; Rämö et al., 1996; Ahl, 1997; Kosunen, 1999; Puura and Flodén, 2000; Selonen et al., 2005; Larin, 2009; Sharkov, 2010; Duchesne et al., 2010; Grabarczyk et al., 2023). Their regional distribution is associated with fault-bounded basins and reactivated crustal structures (Puura and Flodén, 1996; Kukkonen and Lauri, 2009; Larin, 2009; Salminen et al., 2021; Grabarczyk et al., 2023; Lahtinen and Kurhila, 2026).

2.2 Estonian basement and structural framework

The Estonian Precambrian basement is unconformably overlain by Ediacaran-Palaeozoic sedimentary rocks and Quaternary deposits (Raukas and Teedumäe, 1997). The peneplained basement surface dips gently southward at ∼ 0.10-0.20°, while sedimentary-cover thickness increases from ∼ 100 m in northern Estonia to as much as 900 m farther south (Kirs et al., 2004, 2009; Soesoo et al., 2004, 2020; Soosalu et al., 2022). Consequently, direct basement exposure is absent, and its geological architecture is reconstructed primarily from drill cores, potential-field data, seismic information, and correlations with exposed Svecofennian terrains in southern Finland and Sweden (Raukas and Teedumäe, 1997; All et al., 2004; Bogdanova et al., 2015; Solano Acosta, 2026).

The basement is subdivided into several structural-petrological domains, including the Tallinn, Alutaguse, Jõhvi, West-Estonian, Tapa, and South-Estonian zones, which are differentiated by lithology, metamorphic grade, and characteristic gravity and magnetic responses (All et al., 2004; Bogdanova et al., 2015; Soesoo et al., 2020; Solano-Acosta et al., 2023, 2025b). The NW-SE-trending PPDZ, ∼ 30 km wide, separates major basement domains and forms an important regional structural reference in western and northern Estonia (Puura and Flodén, 2000; Bogdanova et al., 2015; Soosalu et al., 2022). Its northwestward continuation has been correlated with the Sottunga-Jurmo Shear Zone in Finland and with additional structures within the northern Bergslagen domain (Högdahl et al., 2009; Bogdanova et al., 2015; Nordbäck et al., 2024).

https://doi.org/10.5194/egusphere-2026-6609
Preprint. Discussion started: 4 November 2026
© Author(s) 2026. CC BY 4.0 License.

2.3 Estonian Rapakivi granitoids

Most Estonian Rapakivi bodies are pink, medium- to coarse-grained, microcline-megacrystic syeno- to monzogranites and commonly contain late aplitic or microsyenitic dykes (Soesoo and Niin, 1992; Soesoo, 1993; Kivisilla et al., 1999; Kirs et al., 2004). Biotite is the dominant mafic mineral, while hornblende also occurs in the Märjamaa, Naissaare, and Neeme intrusions (Kirs et al., 1991; Soesoo and Niin, 1992; Soesoo, 1993; Klein et al., 1994). Despite their broadly similar Rapakivi affinity, these intrusions differ markedly in their internal petrographic organisation and phase development (Potagin, 2024; Solano-Acosta et al., 2026a, c).

The Neeme intrusion, dated to ~ 1.63 Ga (Soesoo and Hade, 2012), is a 25×20 km pluton that extends partly beneath the Gulf of Finland (Fig.1b3). It consists mainly of coarse- to medium-grained, pinkish-grey porphyritic granite cut by aplite and microsyenite dykes. Two melanocratic, locally granodioritic bodies occur in the central and northeastern parts and correspond to Phases Ia and Ib; the remainder of the intrusion is comparatively leucocratic. Partly assimilated gneiss xenoliths are common, and trachytic fabrics occur locally (Soesoo and Niin, 1992; Klein et al., 1994). The mineral assemblage comprises quartz (20-25%), microcline (35-45%), plagioclase (oligoclase-andesine; 15-25%), and biotite (2-10%), with minor hornblende and muscovite. Accessory minerals include apatite, fluorite, titanite, zircon, epidote, and opaque phases (Soesoo and Niin, 1992; Kirs et al., 2004).

The Märjamaa-Kloostri system is the largest Rapakivi intrusion in northern Estonia. It forms an asymmetrically rounded 40×25 km composite pluton in the West-Estonian domain (Fig.1b4) (All et al., 2004; Kirs et al., 2004; Solano-Acosta et al., 2023). Petrographic, geochemical, and geophysical data distinguish three phases (Klein et al., 1994; Solano-Acosta et al., 2025a, 2026c). Earlier U-Pb zircon analyses of Phase I material from drill core 302 yielded an upper-intercept age of 1626 ± 13 Ma (Rämö et al., 1996). Subsequent analyses refined the Phase I age to 1626 ± 3 Ma in drill core 305 and yielded an age of 1629.7 ± 4.2 Ma for Phase III material from Kloostri drill core F323 (Potagin, 2024). Phase I forms a central melanocratic granodiorite rich in gneiss xenoliths; Phase II is a marginal, K-feldspar-rich biotite-hornblende granite; and Phase III is the northwestern Kloostri Na-rich leucogranite, characterised by albite, minor muscovite and fluorite, and locally trachytoid texture (Soesoo and Niin, 1992; Klein et al., 1994; Laitakari et al., 1996). Typical modal proportions are quartz (20-30%), microcline and plagioclase (20-40% each), and biotite (2-10%). Hornblende is restricted to Phases I-II, while magnetite, ilmenite, zircon, apatite, titanite, fluorite, and epidote occur as accessory minerals (Soesoo and Niin, 1992; Kirs et al., 2004).

The Naissaare intrusion has an upper-intercept U-Pb zircon age of 1624 ± 10 Ma, based on Phase I material from drill core 327 (Rämö et al., 1996). The pluton also extends partly beneath the Gulf of Finland and shows lateral variation (Puura and Flodén, 1999, 2000). It is dominated by porphyritic granite cut by aplite and microsyenite veins and comprises two compositionally distinct phases (Fig.1b5): a marginal melanocratic granite with occasional hornblende, and a central leucocratic granite with locally developed trachytoid fabric, post-magmatic muscovite and fluorite, and petrographic affinity to the Kloostri leucogranite (Soesoo and Niin, 1992; Klein et al., 1994). The rocks contain quartz (25-35%), microcline (35-45%), oligoclase plagioclase (20-25%), and biotite; apatite, titanite, zircon, epidote, magnetite, and ilmenite occur as accessory phases (Soesoo and Niin, 1992; Kirs et al., 2004).

https://doi.org/10.5194/egusphere-2026-6609
Preprint. Discussion started: 4 November 2026
© Author(s) 2026. CC BY 4.0 License.

3 Datasets

This study utilised potential-field datasets provided by the Estonian Geological Service. The datasets are publicly observable through the Estonian Geological Survey (EGT) web platform, and can be downloaded from https://gis.egt.ee/geoportaal/ruumiandmed, and include Bouguer anomaly data (Fig.2a) and magnetic anomaly data (Fig.2b). For the present study, both datasets were clipped over a common regional domain of $\sim 75 \times 75$ km, encompassing the Märjamaa-Kloostri, Naissaare, and Neeme intrusions and the intervening sector of the PPDZ (Fig.1b). All potential data were processed using the Universal Transverse Mercator (UTM) coordinate system, specifically UTM Zone $34°$N.

The Bouguer anomaly (Fig.2a) provides insights into subsurface density variations, aiding in the identification of geological structures, crustal thickness, and rock types based on their density (Oja et al., 2021; Osagie et al., 2021; Solano-Acosta et al., 2023; Senger et al., 2025). Gravimetric data, compiled by various institutions since the mid-20^{th} century, were consolidated by the Estonian Land Board and Geological Survey. This dataset covers an area of $74,480$ km^2 and includes $10,882$ measurement points, resulting in an average density of 0.15 points per km^2 (Maasik, 1959; Jürgenson, 2001, 2003; All et al., 2004; All and Gromov, 2005; Oja et al., 2019, 2021) .

The magnetic anomaly (Fig.2b) reveals variations in the concentration of magnetic minerals and provides further insights into crustal structure and composition (Omietimi et al., 2021; Saada et al., 2021; Solano-Acosta et al., 2023). In Estonia, aeromagnetic surveys were conducted throughout the 20^{th} century with a resolution of $1:25,000$ on land and $1:50,000$ offshore from 1987 to 1992 (All et al., 2004; Soesoo et al., 2020). The data were reduced to the $DGRF$-65 anomaly level (Korhonen et al., 2002) with a resolution of 1×1 km^2 (All et al., 2004).

https://doi.org/10.5194/egusphere-2026-6609
Preprint. Discussion started: 4 November 2026
© Author(s) 2026. CC BY 4.0 License.

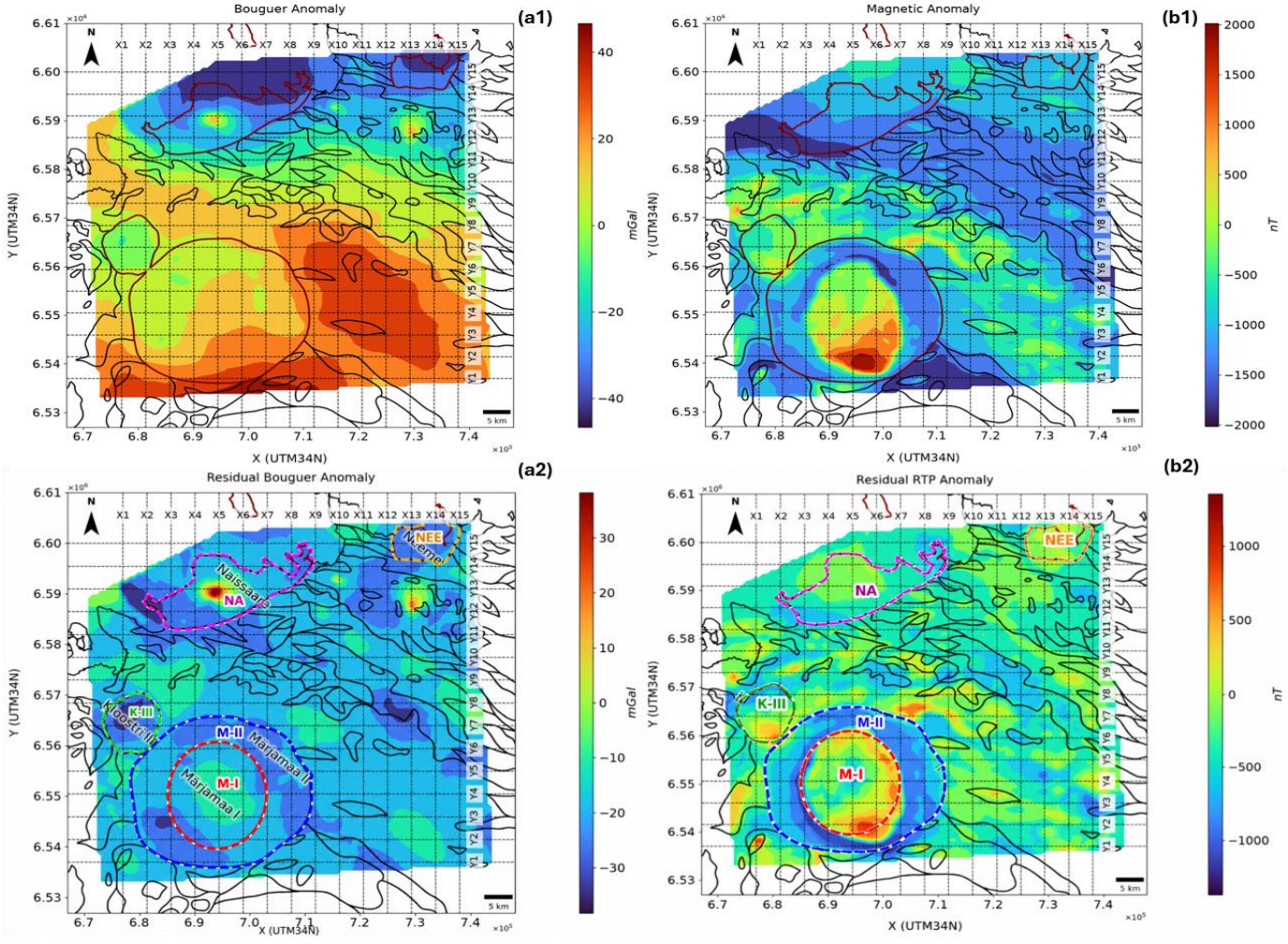


Figure 2. Regional Bouguer gravity and magnetic anomaly maps used for the geophysical analysis. **(a1)** Bouguer anomaly, **(a2)** residual Bouguer anomaly, **(b1)** magnetic anomaly, and **(b2)** residual reduction-to-pole (RTP) magnetic anomaly. Black outlines indicate the mapped basement and redish ones indicate the Rapakivi intrusive boundaries. The locations of the 15 X-oriented and 15 Y-oriented profiles used for the subsequent profile analysis and 3-D inversion assessment are also shown on the maps. Residual maps were the ones used for the inversion (Fig.4). Gravity values are expressed in mGal and magnetic values in nT.

https://doi.org/10.5194/egusphere-2026-6609
Preprint. Discussion started: 4 November 2026
© Author(s) 2026. CC BY 4.0 License.

4 Methodology and results

4.1 Gravity and magnetic processing

Following the workflow of Solano-Acosta et al. (2025a), the Bouguer gravity and magnetic datasets were processed in MAGMAP within Geosoft Oasis montaj to separate long- and short-wavelength potential-field components (Mickus et al., 1991; Geosoft, 2004; Solano-Acosta et al., 2023; Lowrie and Fichtner, 2020). Before spectral filtering, the magnetic anomaly grid was transformed using reduction-to-the-pole (RTP) to approximately centre anomalies over their causative sources (Baranov and Naudy, 1964). The RTP transformation used IGRF-derived parameters for the study-area centroid ($\sim 59.209°$N, $24.644°$E) and the 1992 reference epoch, yielding an inclination of approximately $71.7°$ and a declination of $5.8°$E (Finlay et al., 2010; Omietimi et al., 2021; Solano-Acosta et al., 2023, 2025a) (Fig.3c1).

The complete Bouguer and RTP grids were then separated into regional and residual components using Fourier-domain high- and low-pass filters. Radially averaged power spectra were used to identify the principal wavelength transition (Fig.S1). A cutoff wavenumber of 0.04 cycles/km was adopted: lower wavenumbers represent longer-wavelength regional contributions, while higher wavenumbers emphasise shorter-wavelength density and magnetic-susceptibility variations (Phillips, 2001; Osagie et al., 2021; Saada et al., 2021; Solano-Acosta et al., 2026b). The resulting regional and residual fields are shown in Figures 3a1-a2,c2-c3.

A pseudo-gravity transformation was also calculated from the RTP magnetic field using a fast Fourier transform and Poisson's relation. This provided a gravity-equivalent representation of the magnetic anomaly field for comparison with the Bouguer data (Pratt and Shi, 2004; Geosoft, 2004; Solano-Acosta et al., 2023) (Fig.3a3).

4.2 Derivative analysis

To enhance boundaries and gradients within the residual potential-field datasets, Tilt Derivative Ratio (TDR), Tilt Angle Derivative (TDX), and Analytic Signal (AS) filters were applied to the residual Bouguer and RTP grids (Saada et al., 2021; Solano-Acosta et al., 2023, 2025a). These filters are commonly used to enhance lateral contrasts associated with lithological boundaries, intrusive contacts, and faults (Geosoft, 2004; Osagie et al., 2021; Ibraheem et al., 2018; Ndikum and Tabod, 2024). TDR and TDX emphasise changes in density and magnetisation gradients, whereas the analytic signal highlights the amplitude of the total field gradient and is comparatively insensitive to the direction of magnetisation (Saada et al., 2021). The mathematical definitions of the applied derivatives are provided in Figure 3.

4.3 Upward continuation

Upward continuation (UC) was applied to the residual Bouguer and RTP datasets to evaluate the persistence of potential-field anomalies with increasing continuation height and to progressively suppress shorter-wavelength contributions associated with shallow sources (Blakely, 1995; Saibi et al., 2006; Ganiyu et al., 2013; Okpoli and Akingboye, 2019).

https://doi.org/10.5194/egusphere-2026-6609
Preprint. Discussion started: 4 November 2026
© Author(s) 2026. CC BY 4.0 License.

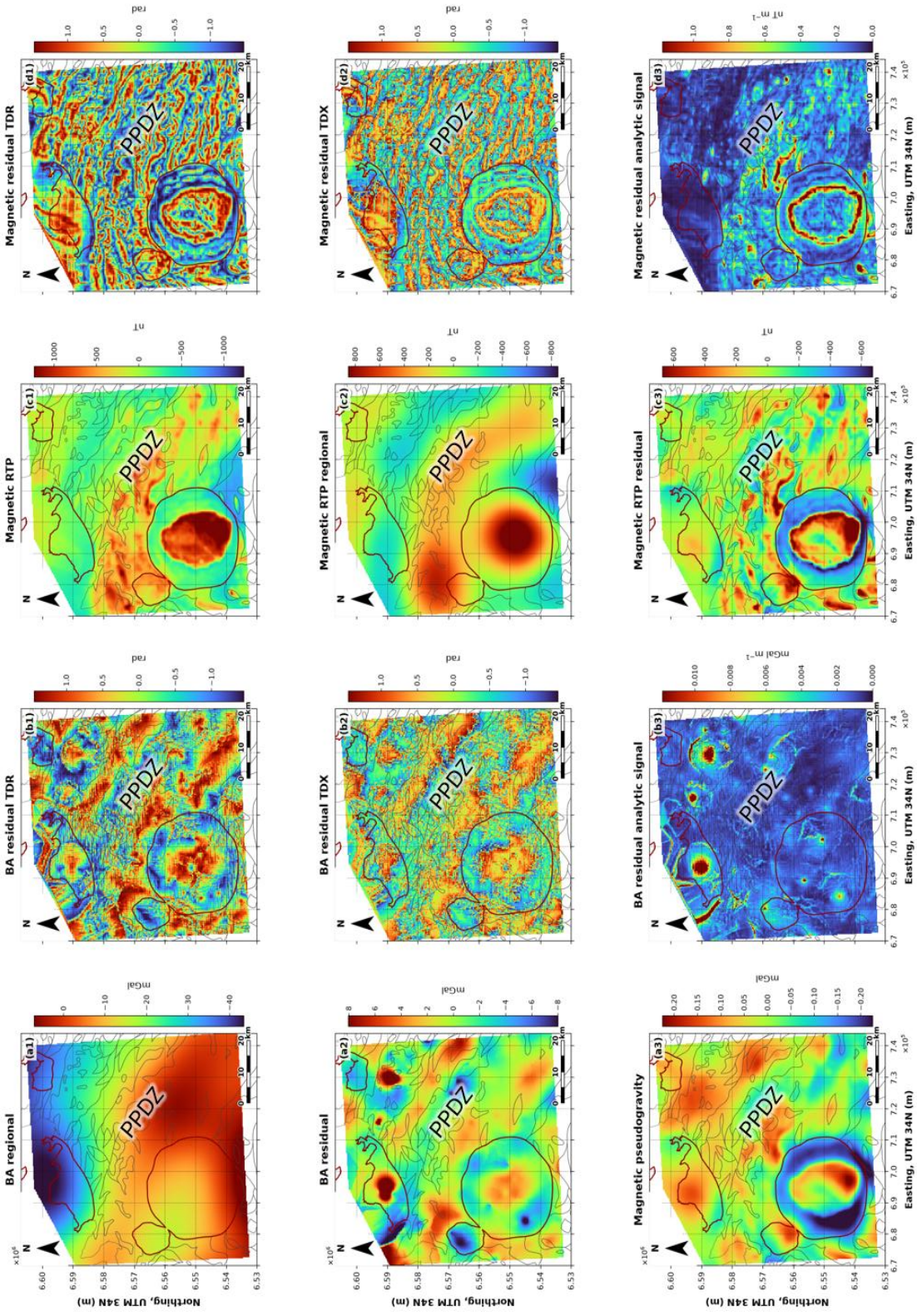


Figure 3. Geophysical regional and residual wave-cut, and residual derivative results. (a) Bouguer maps: (a1) regional component, (a2) residual anomalies (cut at 0.04 cycles/km; Fig.S1), (a3) pseudo-gravity transformation derived from the RTP magnetic map. (b) Bouguer residual derivatives: (b1) Tilt Derivative Ratio (TDR), defined as $\tan^{-1}\left(\frac{\partial f/\partial z}{\sqrt{(\partial f/\partial x)^2+(\partial f/\partial y)^2}}\right)$; (b2) Tilt Angle Derivative (TDX), defined as $\tan^{-1}\left(\frac{\sqrt{(\partial f/\partial x)^2+(\partial f/\partial y)^2}}{\partial f/\partial z}\right)$; (b3) Analytic Signal (AS), defined as $\sqrt{\left(\frac{\partial f}{\partial x}\right)^2+\left(\frac{\partial f}{\partial y}\right)^2+\left(\frac{\partial f}{\partial z}\right)^2}$. Potential field derivatives are calculated in the X, Y, and Z directions. (c) Magnetic reduction-to-the-pole (RTP) maps: (c1) RTP magnetic anomaly, (c2) regional field, and (c3) residual anomaly. (d) RTP residual derivatives: (d1) TDR, (d2) TDX, and (d3) AS. Granitic bodies are outlined by reddish contours.

https://doi.org/10.5194/egusphere-2026-6609
Preprint. Discussion started: 4 November 2026
© Author(s) 2026. CC BY 4.0 License.

In the frequency domain, upward continuation can be expressed as $F_\zeta(p,q) = e^{-\zeta\sqrt{p^2+q^2}} F_0(p,q)$, where $F_0(p,q)$ is the Fourier transform of the field at the observation surface, ζ is the continuation height, and $F_\zeta(p,q)$ is the upward-continued field.

Following the principles discussed by Jacobsen (1987), the progressive attenuation of anomalies with continuation height was used qualitatively to evaluate the wavelength and depth persistence of the observed gravity and magnetic signals. Upward continuation was calculated from 500 to 15,500 m at 1,000 m intervals for both residual Bouguer and RTP datasets (Fig.S2). Because upward continuation represents filtering rather than a direct depth inversion, the disappearance of an anomaly is interpreted as a measure of signal persistence with height, rather than as the absolute depth of the causative source (Ganiyu et al., 2013).

4.4 SimPEG inversion

Three-dimensional joint inversion of the residual Bouguer gravity and RTP magnetic datasets (Figs.3a2,b2) was carried out using the SimPEG Python framework (Cockett et al., 2015). The cross-gradient joint inversion SimPEG method was used to encourage spatial correspondence between density-contrast and magnetic-susceptibility structures while allowing the two physical-property models to retain independent amplitudes. Joint potential-field inversion using this approach has been successfully applied to igneous, hydrothermal, and structurally complex geological systems (Miller et al., 2017; Ardestani et al., 2021; Ardestani, 2022; Mitchell et al., 2023; Solano-Acosta et al., 2025a).

The regional inversion domain extended from 670,000 to 746,000 m E and from 6,532,000 to 6,606,000 m N in UTM Zone 34N, with the vertical model extending from $-15,000$ to $+200$ m. The tensor mesh comprised $38 \times 37 \times 19$ cells, corresponding to a total of 26,714 cells. Horizontal cell dimensions were 2,000 m in both the X and Y directions, while the vertical cell thickness was 800 m. The mesh origin was located at $(670000,\ 6532000,\ -15000)$ m. This configuration provided a regional model volume extending to a depth of 15 km, consistent with the maximum depth range examined in the upward-continuation analysis (Fig.S2). Figure S3 shows the mesh grid with observed, predicted, and misfit responses.

Thirty vertical cross-sections were extracted from the final inversion models, comprising 15 X-oriented profiles (X_{1-15}) and 15 Y-oriented profiles (Y_{1-15}). Their locations are shown in Figure 2. These sections were used to examine the lateral and vertical distributions of density contrast and magnetic susceptibility across the Märjamaa-Kloostri, Naissaare, and Neeme granitoids, as well as the surrounding basement. Background values were set to 1×10^{-3} g cm^{-3} for density contrast and 1×10^{-3} SI for magnetic susceptibility as done in Solano-Acosta et al. (2025a). The corresponding gravity and magnetic inversion sections are presented in Figure 4.

https://doi.org/10.5194/egusphere-2026-6609
Preprint. Discussion started: 4 November 2026
© Author(s) 2026. CC BY 4.0 License.

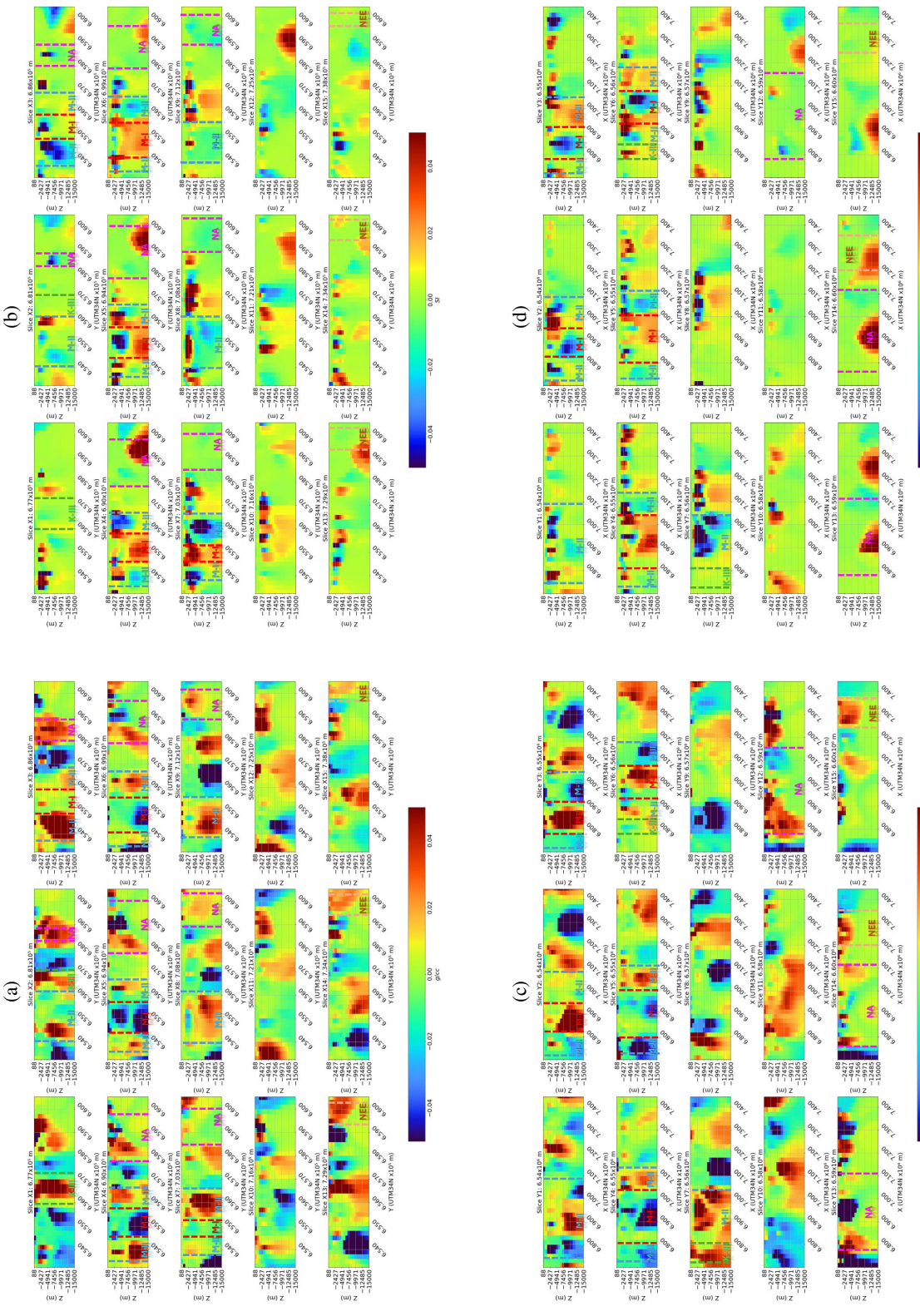


Figure 4. SimPEG inversion results for the residual Bouguer gravity and reduction-to-the-pole (RTP) magnetic datasets. The inversion models are presented along the 15 X-oriented and 15 Y-oriented profiles shown in Figure 2. **(a)** Bouguer density-contrast inversion along the X profiles; **(b)** magnetic-susceptibility inversion along the X profiles; **(c)** Bouguer density-contrast inversion along the Y profiles; and **(d)** magnetic-susceptibility inversion along the Y profiles. Coloured dashed boundaries and arrows indicate the approximate intersections of the mapped Rapakivi bodies with each profile: M-I, Märjamaa Phase I; M-II, Märjamaa Phase II; K-III, Kloostri Phase III; NA, Naissaare; and NEE, Neeme. These limits are intended as spatial guides based on the mapped granitoid boundaries shown in Figure 1, after Klein et al. (1994). The sections illustrate the lateral and vertical variations in density contrast and magnetic susceptibility beneath and around the investigated Estonian Rapakivi intrusions.

https://doi.org/10.5194/egusphere-2026-6609
Preprint. Discussion started: 4 November 2026
© Author(s) 2026. CC BY 4.0 License.

4.5 Three-dimensional model visualisation

The 3-D representation of the recovered density-contrast and magnetic-susceptibility models (Fig.5) highlights the heterogeneous spatial distribution of the principal petrophysical anomalies across the Estonian Rapakivi intrusions. The selected high- and low-contrast domains delineate distinct subsurface patterns, with differences in their lateral extent, apparent vertical continuity, and spatial correspondence between density and magnetic susceptibility. Particularly pronounced magnetic contrasts occur in deeper portions of some modelled domains, whereas other intrusions exhibit more restricted vertical expressions. The Märjamaa and Kloostri systems display locally tabular arrangements of contrasting physical-property domains, with Kloostri appearing more spatially discrete, while Naissaare and Neeme exhibit comparatively shallower expressions of the selected anomalies. These relationships are illustrated from two opposing perspectives in Figure 5, with the corresponding interactive three-dimensional models provided within Supplementary File.

To examine physical-property variations associated with the mapped Rapakivi intrusions, the recovered model cells were spatially filtered according to whether their horizontal cell centres occurred within the corresponding intrusion polygons. For each physical property, the 15th and 85th percentiles (P15 and P85) were calculated from the valid recovered values within these footprints. Only cells with values $\leq$P15 or $\geq$P85 were displayed, allowing the lower and upper tails of the recovered distributions to be examined while excluding intermediate values. Density contrasts were represented using a blue-to-red colour scale, whereas magnetic susceptibility was displayed using a green-to-orange scale. Separate density and susceptibility representations, together with their combined visualisation, were generated to evaluate the spatial distribution and correspondence of the recovered anomalies. Importantly, the displayed volumes represent percentile-selected model cells within the vertically projected intrusion footprints, rather than independently constrained three-dimensional intrusion boundaries.

https://doi.org/10.5194/egusphere-2026-6609
Preprint. Discussion started: 4 November 2026
© Author(s) 2026. CC BY 4.0 License.

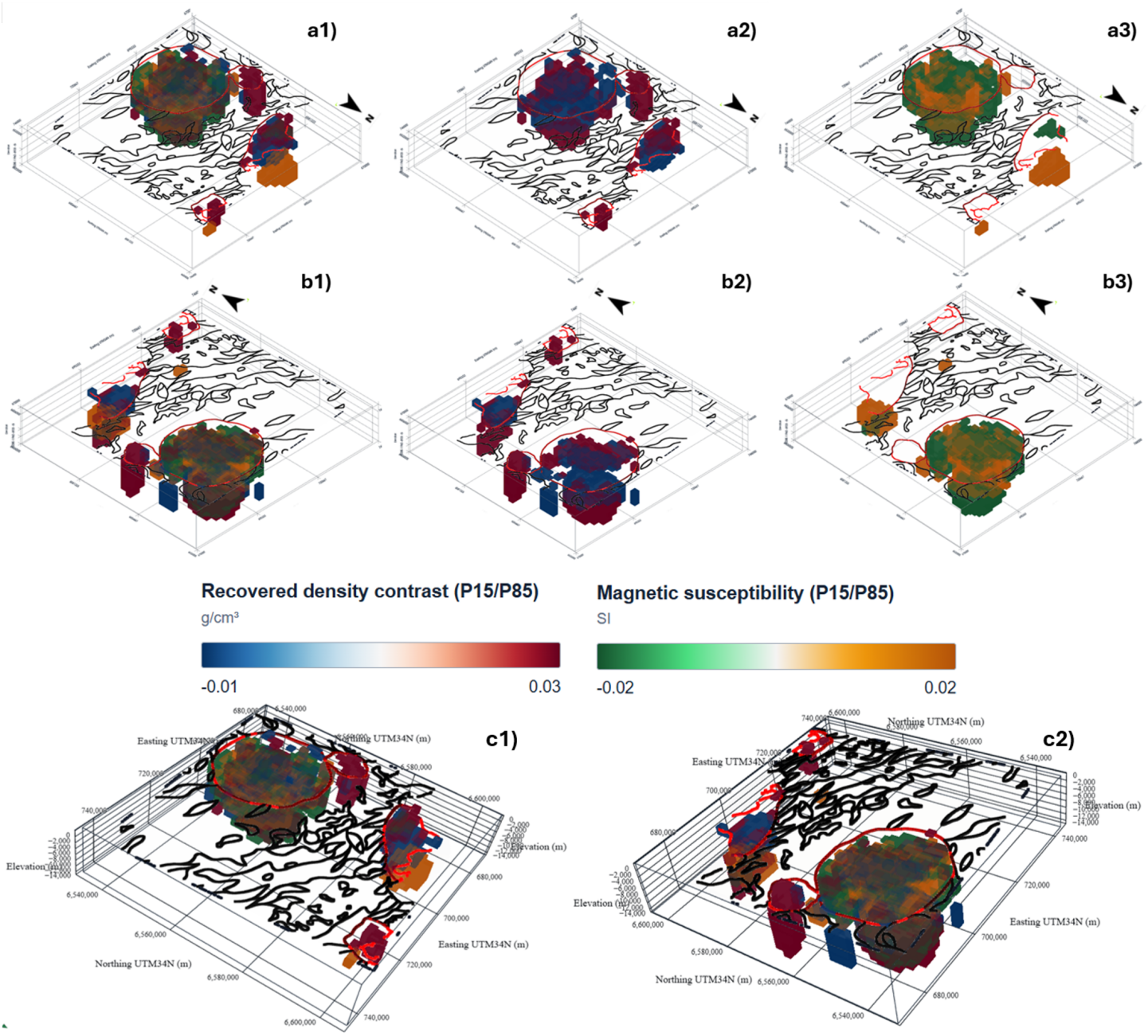


Figure 5. 3-D visualisation of recovered density-contrast and magnetic-susceptibility models for the Estonian Rapakivi intrusions. Complementary views are shown at azimuths of 45° (a1–a3) and 225° (b1–b3), both at 40° elevation. Panels (a1,b1) show combined distributions; (a2,b2) show density contrasts (blue: lower; red: higher); and (a3,b3) show magnetic susceptibility (green: lower; orange: higher). Panels (c1,c2) enlarge the combined models, showing relationships between petrophysical domains and regional geological structures. Only cells within mapped intrusion footprints and in the lower ($\leq P_{15}$) or upper ($\geq P_{85}$) percentiles of each petrophysical property are displayed. Black lines mark mapped geological boundaries; red outlines indicate intrusion surface extents. Coordinates use WGS 84/UTM zone 34N (EPSG:32634); elevation is in metres, density contrast in g/cm^3, and susceptibility in SI units. Volumes show selected property contrasts, not independently constrained lithological contacts or subsurface intrusion boundaries. Interactive 3-D HTML models are available in the Supplementary Material.

https://doi.org/10.5194/egusphere-2026-6609
Preprint. Discussion started: 4 November 2026
© Author(s) 2026. CC BY 4.0 License.

5 Discussion

5.1 Regional potential-field architecture and the PPDZ

The derivative maps show a consistent NW-SE alignment of gravity and magnetic gradients, broadly subparallel to the Paldiski-Pskov Deformation Zone (PPDZ) (Fig.3c1). This trend is especially clear in the TDR and TDX derivative products, where elongated gradient corridors reflect the regional structural arrangement of the crystalline basement. This correspondence supports previous interpretations of the PPDZ as a long-lived crustal discontinuity inherited from the Palaeoproterozoic Svecofennian basement and later reactivated during tectonic and magmatic events (Nordbäck et al., 2024; Solano-Acosta et al., 2025a; Solano Acosta, 2026; Lahtinen and Kurhila, 2026). The coherent expression of these gradients in both gravity and magnetic datasets provides further evidence for the regional persistence of this structural framework.

The analytic-signal (AS) products (Fig.3b3,d3) further highlight contrasts in the distribution and intensity of petrophysical boundaries. In the residual Bouguer field, high-amplitude responses occur locally as narrow, spatially confined lineations that do not consistently follow the mapped margins of the Rapakivi intrusions. Similar features in the Märjamaa-Kloostri area have previously been interpreted as possible feeder zones, mafic or anorthositic dykes, or other high-density subsurface contacts (Solano-Acosta et al., 2025a). Märjamaa-Kloostri and Naissaare are comparatively well expressed in the Bouguer AS, with particularly pronounced amplitudes around Naissaare, whereas Naissaare has a substantially weaker magnetic AS response. Conversely, the residual reduced-to-the-pole (RTP) magnetic AS shows stronger gradients within and around Märjamaa-Kloostri, particularly west of and near the PPDZ. Neeme is less distinctly expressed in both datasets. These differences indicate that the principal density and magnetic boundaries do not systematically coincide, reflecting contrasting petrophysical characteristics among the investigated intrusive systems.

5.2 Contrasting subsurface architectures and petrophysical differentiation

The SimPEG joint potential-field inversion reveals substantial differences in the recovered subsurface geometries of Märjamaa-Kloostri, Naissaare, and Neeme (Fig.4). Density contrasts generally define shallower, more internally heterogeneous domains, while positive magnetic-susceptibility structures tend to show greater apparent vertical continuity, in some cases extending towards the lower boundary of the 15 km model. Their distinct spatial patterns suggest that density and magnetic susceptibility provide complementary constraints on the physical-property architecture of the intrusive systems, rather than defining identical subsurface geometries.

In the Märjamaa-Kloostri area (Fig.1b4), the regional inversion extends the local-scale modelling of Solano-Acosta et al. (2025a), which investigated the system to approximately 10 km depth. The present results indicate that Märjamaa Phases I and II comprise several vertically stacked or block-like domains, whose widths and lateral positions vary with depth, as shown by profiles X_{3-6} (Figs.4a and 4b). The recovered density structure includes both positive and negative contrasts, whereas magnetic-susceptibility anomalies show a more pronounced vertical organisation and extend towards the lower model boundary. By comparison, Kloostri Phase III has a relatively discrete, locally tabular geometry, with shallower and less pronounced magnetic contrasts, particularly along profiles Y_{6-7} (Fig.4d). These relationships suggest that Märjamaa and Kloostri comprise

https://doi.org/10.5194/egusphere-2026-6609
Preprint. Discussion started: 4 November 2026
© Author(s) 2026. CC BY 4.0 License.

distinct intrusive compartments, despite being associated with a broader magmatic system. The shallow concentric arrangement of Märjamaa remains consistent with the piston-cauldron geometry proposed by Solano-Acosta et al. (2025a), while the deeper recovered anomalies indicate a more heterogeneous architecture than the shallow structural expression alone suggests. However, because magnetic contrasts continue towards 15 km, the full vertical extent of the associated sources cannot be established.

Naissaare has a different configuration, with a relatively heterogeneous shallow density structure and a more coherent, vertically developed magnetic response (Fig.4). The petrographic subdivision into Phases I and II, mapped by Klein et al. (1994) and Solano-Acosta et al. (2026a), is not expressed as two sharply separated geophysical domains (Fig.1b5). Phase II shows comparatively lower-amplitude, shallower density contrasts towards the Baltic-facing side of the intrusion, whereas Phase I is associated with stronger positive density contrasts that extend to greater depths, as illustrated by profile X_5 (Fig.4a). In addition, profile Y_{12} (Fig.4d) shows a lateral offset between the mapped upper intrusion and the deeper magnetic-susceptibility structure. The latter's relatively steep margins and vertical continuity are compatible with a block-like or columnar geophysical geometry, potentially involving an inclined feeder-related continuation rather than a simple, vertically aligned plutonic body (Cruden, 1998; Grocott et al., 1999; Karell et al., 2014). Nevertheless, the magnetic anomaly does not uniquely identify a magma conduit, and its relationship to the shallower density structure remains interpretative.

Neeme (Fig.1b3) has a smaller, generally lower-contrast geophysical expression. Its positive density anomaly forms a relatively shallow body, approximately centred beneath the mapped intrusion, particularly along profile X_{14} (Fig.4a). The corresponding magnetic-susceptibility model, however, shows a deeper, laterally displaced structure (Fig.4b), indicating that the distribution of magnetic material cannot be represented solely by the recovered shallow density geometry. The petrographic Phases Ia, Ib, and II described by Klein et al. (1994) are not individually resolved at the present model scale. The deeper magnetic response could reflect a relatively magnetite-rich intrusive component, a mafic-associated body, or a magnetised basement contact (Vigneresse, 2005; Bonin, 2007; Dall'Agnol et al., 2012; Johansson et al., 2016). Accordingly, its apparent vertical persistence should not be interpreted directly as a downward continuation of the exposed granitoid intrusion.

The three-dimensional comparison of the recovered density and magnetic-susceptibility contrasts (Fig.5) provides a complementary perspective on these relationships. The spatially selected high- and low-value domains highlight differences in lateral distribution, internal heterogeneity, and apparent vertical organisation among the intrusions. Particularly pronounced magnetic contrasts in deeper parts of some modelled domains may reflect variations in magnetic-mineral abundance, oxidation state, or contributions from Fe-rich lithologies. These may include magnetite-bearing mafic components or Fe-Ti-oxide-enriched assemblages associated with the broader anorthosite-mangerite-charnockite-granite (AMCG) association (Ahl, 1997; Kirs et al., 2004; Rämö and Haapala, 2005; Vigneresse, 2005; Larin, 2009; Sharkov, 2010; Dall'Agnol et al., 2012; Solano-Acosta et al., 2025a, 2026c). However, magnetic susceptibility alone cannot establish an anorthositic or other specific mafic composition. In addition, the displayed P15/P85 volumes represent selected recovered physical-property contrasts, not independently constrained lithological contacts or intrusive roots.

The correspondence between mapped magmatic phases and geophysical domains also varies among the studied intrusions. Märjamaa-Kloostri shows the clearest relationship between its mapped subdivisions and internal petrophysical structure,

https://doi.org/10.5194/egusphere-2026-6609
Preprint. Discussion started: 4 November 2026
© Author(s) 2026. CC BY 4.0 License.

whereas Naissaare's two phases are only partially distinguishable and Neeme's remain unresolved. Thus, petrographic and geochemical differentiation (Soesoo and Niin, 1992; Soesoo, 1993; Klein et al., 1994; Potagin, 2024; Solano-Acosta et al., 2026c; Solano-Acosta, 2026) does not necessarily yield corresponding density or magnetic-susceptibility domains at the resolution of the present inversion. This underscores the importance of integrating petrological and mineralogical evidence when interpreting the physical-property distribution of individual Rapakivi intrusions.

5.3 Tectonomagmatic implications for the PPDZ-hosted Rapakivi system

The contrasting architectures identified across the Estonian Rapakivi intrusions suggest that regional tectonic inheritance and local emplacement processes exerted complementary, though not necessarily equivalent, controls on their development. Although the PPDZ is an important inherited crustal structure that may have favoured magma ascent and localisation, the recovered intrusion geometries show no systematic elongation parallel to its NW-SE orientation. Moreover, Märjamaa-Kloostri, Naissaare, and Neeme remain geophysically distinct systems, with no continuous density- or magnetic-susceptibility structure connecting them at the resolution and depth range investigated (Figs.4,5). Thus, previously proposed deeper connections or shared magma-transfer pathways (Nordbäck et al., 2024; Solano-Acosta et al., 2025a) remain regional tectonomagmatic hypotheses, rather than features demonstrated by the present inversion. The plutons' common affiliation with the Wiborg magmatic suite therefore does not imply identical emplacement geometries, magma-supply configurations, or evolutionary histories.

The heterogeneous architecture of Märjamaa-Kloostri can be interpreted in the context of the transtensional pull-apart and piston-cauldron emplacement model proposed by Solano-Acosta et al. (2025a). In this model, dextral transtensional reactivation along inherited Svecofennian structures facilitated magma ascent, intrusive accommodation, and successive phases of cauldron subsidence. The present regional results suggest that similar structural processes may have operated within a more extensive, internally compartmentalised magmatic framework, potentially involving multiple emplacement centres and deeper magma-transfer or storage zones. Kloostri's relatively discrete geometry and Märjamaa's heterogeneous deeper architecture are consistent with different levels or stages of magma accommodation within such a framework. However, the inversion does not establish a single, continuous ring-cauldron structure beneath the investigated plutons. The earlier model may therefore describe a local expression of a broader transtensional system without necessarily defining the emplacement mechanism of every associated intrusion.

This interpretation is consistent with the Palaeoproterozoic structural inheritance of the PPDZ, where Svecofennian fabrics and Riedel-type fracture arrangements have been linked to Mesoproterozoic transtensional reactivation (Solano-Acosta et al., 2025a; Solano Acosta, 2026). Petrogenetic investigations likewise place the Estonian Rapakivi suites in an extensional to continental-rift-related tectonic setting (Solano-Acosta et al., 2026c; Solano-Acosta, 2026). More broadly, Fennoscandian A-type and AMCG magmatism has been associated with lithospheric extension, mantle upwelling, and the tectonic reorganisation and fragmentation of Nuna (Pirajno and Santosh, 2015; Salminen et al., 2021; Lahtinen and Kurhila, 2026). In this context, the PPDZ may have acted as a crustal-scale zone of weakness that facilitated melt migration, while local magma supply, host-rock rheology, structural accommodation, and successive intrusive pulses shaped the architecture of individual

https://doi.org/10.5194/egusphere-2026-6609
Preprint. Discussion started: 4 November 2026
© Author(s) 2026. CC BY 4.0 License.

plutons. These processes are consistent with multi-level models of A-type and Rapakivi magmatism involving magma transfer, storage, and emplacement at different crustal levels (Bonin, 2007; Sharkov, 2010; Johansson, 2023). Nevertheless, the present inversion cannot uniquely distinguish among alternative deep magmatic configurations or establish the lithological identity of the recovered magnetic sources.

The deeper crustal and thermal framework described by Solano-Acosta et al. (2023) provides further context for regional differences among these intrusive systems. Variations in Moho depth, Conrad discontinuity, Curie-point depth, and heat flow broadly correspond to the distribution of the Estonian Rapakivi intrusions (Fig.1c-f). Märjamaa-Kloostri is associated with comparatively shallow crustal and thermal boundaries and elevated heat flow; Naissaare occupies an intermediate setting; and Neeme lies in a region characterised by deeper boundaries and relatively lower heat flow. These spatial relationships may reflect variations in crustal thickness, inherited structural configurations, and lithospheric thermal evolution. Because the regional boundaries extend below the inversion's 15 km depth range, they may provide context for deeper crustal heterogeneity, but they do not demonstrate that individual granitoid bodies extend to the Moho, Conrad discontinuity, or Curie-point depths .

Post-magmatic erosion, exhumation, and tectonic reorganisation may also have modified the intrusions' presserves as an inherited structural corridor despite the intrusions' differing geometries. Puura and Flodén (1999) argued that erosion alone could not account for the approximately 10-15 km of inferred crustal thinning and proposed an additional contribution from regional uplift and thermal processes. Puura and Flodén (2000) considered differential erosion and tectonic tilting, estimating approximately 5-10 km of crustal removal, whereas Sharkov (2010) proposed more extensive erosion of approximately 16-20 km. Despite their differences, these estimates collectively indicate substantial post-orogenic crustal reworking. Accordingly, the contrasting preserved geometries of Märjamaa-Kloostri, Naissaare, and Neeme may reflect both original emplacement conditions and subsequent differences in exhumation, tilting, and preservation of intrusive levels.

The inferred petrophysical architecture also has implications for the metallogenic potential of Rapakivi-related systems (Fig.4), although mineral exploration is not the principal objective of this study. Mantle-driven extension, lithospheric thinning, and mafic magma contributions associated with A-type and AMCG magmatism have been linked to geological settings favourable for IOCG, Sn-W-Mo, Cu-Au-U, and REE mineralisation (Vigneresse, 2005; Bonin, 2007; Dall'Agnol et al., 2012; Pirajno and Santosh, 2015; Salminen et al., 2021). Inherited crustal-scale structures may promote magma and fluid migration, while F-rich assemblages and brittle deformation can contribute to the mobilisation and redistribution of HFSE, REE, and associated metals (Vigneresse, 2005; Bonin, 2007; Pirajno and Santosh, 2015; Valkama et al., 2016; Siachoque et al., 2017). Märjamaa Phase I is particularly relevant in this context: its heterogeneous and vertically extensive geophysical architecture coincides with previously documented Fe-P-REE enrichment (Potagin, 2024; Solano Acosta, 2026). Although this association does not establish a direct genetic link between the recovered anomalies and mineralisation, it identifies an area where further petrophysical, mineralogical, and geochemical investigation could be especially informative. Potential-field anomalies extending beyond mapped granitoid boundaries may also provide targets for investigating concealed lithological or structural features.

Overall, the combined potential-field and three-dimensional models support a common regional tectonomagmatic framework comprising several geometrically and petrophysically distinct intrusive systems, rather than a single, continuously re-

https://doi.org/10.5194/egusphere-2026-6609
Preprint. Discussion started: 4 November 2026
© Author(s) 2026. CC BY 4.0 License.

solved batholithic body. The PPDZ may have provided the inherited structural framework for magma localisation, while local emplacement conditions and subsequent crustal modification shaped each intrusion's final architecture. Extending previous geological and geophysical interpretations of Estonian Rapakivi magmatism (Soesoo and Niin, 1992; Soesoo, 1993; Klein et al., 1994; Puura and Flodén, 1996, 1999, 2000; All et al., 2006; Kirs et al., 2004; Potagin, 2024; Solano-Acosta et al., 2025a, 2026c; Solano-Acosta, 2026), the present results provide further constraints on the internal physical-property differentiation, spatial organisation, and apparent depth continuity of Märjamaa-Kloostri, Naissaare, and Neeme.

6 Conclusions

This study extends previous geophysical models of the Märjamaa-Kloostri Rapakivi complex to a regional scale, depths of 15 km, and the Naissaare and Neeme intrusions. It combines gravity and magnetic data, potential-field derivatives, upward-continuation filters, and 3-D SimPEG inversion. The findings associate Estonia's ∼1.6 Ga Wiborg-suite Rapakivi bodies with the northwest-southeast-trending Paldiski-Pskov Deformation Zone (PPDZ), but reveal varied subsurface architectures. Gravity and magnetic gradients mainly follow the PPDZ, suggesting it is an inherited structural corridor despite differing intrusion geometries. Märjamaa has a shallow, concentric structure consistent with the piston-cauldron model, whereas inversion reveals a more complex, vertically extensive, heterogeneous system, with positive magnetic signals to 15 km; as well as for Kloostri, suggesting a multi-level intrusive root and deeper magma-transfer and storage zones.

Naissaare has a distinct strong vertical magnetic feature and variable shallow density, with limited correlation to geophysical phases. Its geometry suggests a vertically extensive intrusive column, possibly including an inclined feeder-related continuation rather than a shallow, closed pluton.

Neeme has the weakest gravity and magnetic contrasts but a deeper magnetic extension, indicating greater vertical extent than gravity data alone suggest. This may reflect a deep feeder-related or more magnetically susceptible component beneath the shallow body.

Overall, the 3-D models show substantial petrophysical heterogeneity, with distinct lateral geometries, variable vertical extent, and locally strong deep magnetic contrasts. The plutons likely formed under different local magmatic and structural conditions within the same regional tectonomagmatic system. Results support a compartmentalised transtensional emplacement framework, potentially involving Fe–Ti oxide-rich mafic components and differentiated intrusive phases, though depth-geochemical anomalies and depth extents remain uncertain. Despite sharing a tectono-magmatic environment, the intrusions developed distinct internal structures shaped by magma emplacement, crustal position, structural conditions, and host-rock rheology. The regional inversion refines the Märjamaa-Kloostri model and provides the first comparable 3-D insights into the hidden architecture and depth continuity of Naissaare and Neeme.

https://doi.org/10.5194/egusphere-2026-6609
Preprint. Discussion started: 4 November 2026
© Author(s) 2026. CC BY 4.0 License.

Supplementary data

Supplementary material is available in the repository and includes interactive three-dimensional geophysical models of the Estonian Rapakivi intrusions. The compressed archive contains interactive HTML visualisations of the recovered density-contrast, magnetic-susceptibility, and combined models, along with geological boundaries and mapped intrusion outlines. Readers can rotate and zoom the visualisations to examine the spatial distribution of the recovered physical-property contrasts from different perspectives. To access the models, extract the ZIP archive and open the relevant main HTML files in a compatible web browser, keeping the associated viewer files in the same directory.

Funding

This research was supported by the DEXPLORE Horizon Research Funds (document number VHE24051) and was funded through the Horizon Europe program HORIZON-CL4-2024-RESILIENCE-01-01. Special thanks to the EU Funding and Tenders Portal for its support, linked to project ID number 101178897.

Disclosure statement

The author states that they have no known competing financial interests or personal ties that may have influenced the work described in this study.

Author contribution

Juan David Solano-Acosta - conceptualization, methodology, data curation, modeling, visualization, interpretation, writing, and editing.

https://doi.org/10.5194/egusphere-2026-6609
Preprint. Discussion started: 4 November 2026
© Author(s) 2026. CC BY 4.0 License.

References

Ahl, M.: Rapakivi Granites and Related Rocks in Central Sweden: 7th International Symposium on Rapakivi Granites, July 24-26 1996, University of Helsinki, Finland: Excursion July 16-23 1996, vol. 87, Sveriges geologiska undersökning, 1997.

All, T. and Gromov, O.: Geoloogilise baaskaardi Vaida(6341) lehe gravimeetrilis e teemakihi täiendamine [Complementing the gravimetric layer of the geological base-map Vaida (6341) sheet], Technical report, Eesti Geoloogiakeskus, EGF, 20 pp., 2005.

All, T., Puura, V., and Vaher, R.: Orogenic structures of the Precambrian basement of Estonia as revealed from the integrated modelling of the crust, in: Proceedings of the Estonian Academy of Sciences, Geology, vol. 53, pp. 165–189, Estonian Academy Publishers, https://doi.org/10.3176/geol.2004.3.03, 2004.

All, T., Flodén, T., and Puura, V.: A complex model of Mesoproterozoic sedimentary and igneous suites in a graben setting north of Gotland, Baltic Sea, GFF, 128, 53–63, https://doi.org/10.1080/11035890601281053, 2006.

Ardestani, V. E.: Sparse norm and Cross-gradient inversions of gravity and magnetic data sets utilizing open-source resources in Python Case study: Hematite ore body in Jalal Abad area (Iran), University of Tehran Press, 2022.

Ardestani, V. E., Fournier, D., and Oldenburg, D. W.: Gravity and magnetic processing and inversion over the Mahallat geothermal system using open source resources in Python, Pure and Applied Geophysics, 178, 2171–2190, https://doi.org/10.1007/s00024-021-02763-6, 2021.

BABEL Working Group: Deep seismic reflection/refraction interpretation of crustal structure along BABEL profiles A and B in the southern Baltic Sea, Geophysical Journal International, 112, 325–343, https://doi.org/10.1111/j.1365-246X.1993.tb01173.x, 1993a.

BABEL Working Group: Integrated seismic studies of the Baltic Shield using data in the Gulf of Bothnia region, Geophysical Journal International, 112, 305–324, https://doi.org/10.1111/j.1365-246X.1993.tb01172.x, 1993b.

Baranov, V. and Naudy, H.: Numerical calculation of the formula of reduction to the magnetic pole, Geophysics, 29, 67–79, https://doi.org/10.1190/1.1439334, 1964.

Blakely, R. J.: Potential Theory in Gravity and Magnetic Applications, Cambridge University Press, Cambridge, UK, https://doi.org/10.1017/CBO9780511549816, 1995.

Bogdanova, S., Gorbatschev, R., Skridlaite, G., Soesoo, A., Taran, L., and Kurlovich, D.: Trans-Baltic Palaeoproterozoic correlations towards the reconstruction of supercontinent Columbia/Nuna, Precambrian Research, 259, 5–33, https://doi.org/10.1016/j.precamres.2014.11.023, 2015.

Bonin, B.: A-type granites and related rocks: evolution of a concept, problems and prospects, Lithos, 97, 1–29, https://doi.org/10.1016/j.lithos.2006.12.007, 2007.

Cockett, R., Kang, S., Heagy, L. J., Pidlisecky, A., and Oldenburg, D. W.: SimPEG: An open source framework for simulation and gradient based parameter estimation in geophysical applications, Computers & Geosciences, 85, 142–154, https://doi.org/10.1016/j.cageo.2015.09.015, 2015.

Cruden, A. R.: On the emplacement of tabular granites, Journal of the Geological Society, 155, 853–862, https://doi.org/10.1144/gsjgs.155.5.0853, 1998.

Dall'Agnol, R., Teixeira, N. P., Rämö, O. T., Moura, C. A. V., Macambira, M. J. B., and de Oliveira, D. C.: Petrogenesis of the Paleoproterozoic rapakivi A-type granites of the Archean Carajás metallogenic province, Brazil, Lithos, 80, 101–129, https://doi.org/10.1016/j.lithos.2004.03.058, 2005.

https://doi.org/10.5194/egusphere-2026-6609
Preprint. Discussion started: 4 November 2026
© Author(s) 2026. CC BY 4.0 License.

Dall'Agnol, R., Frost, C. D., and Ramö, O. T.: IGCP Project 510 "A-type Granites and Related Rocks through Time": Project Vita, Results, and Contribution to Granite Research, Lithos, 151, 1–16, https://doi.org/10.1016/j.lithos.2012.08.003, 2012.

Duchesne, J.-C., Martin, H., Bagin´ski, B., Wiszniewska, J., and Vander Auwera, J.: The origin of ferroan-potassic A-type granitoids: the case of the hornblende–biotite granite suite of the Mesoproterozoic Mazury complex, northeastern Poland, The Canadian Mineralogist, 48, 947–968, https://doi.org/10.3749/canmin.48.4.947, 2010.

Elo, S. and Korja, A.: Geophysical interpretation of the crustal and upper mantle structure in the Wiborg rapakivi granite area, southeastern Finland, Precambrian Research, 64, 273–288, https://doi.org/10.1016/0301-9268(93)90081-C, 1993.

Emslie, R. F.: Anorthosite Massifs, Rapakivi Granites, and Late Proterozoic Rifting of North America, Precambrian Research, 7, 61–98, https://doi.org/10.1016/0301-9268(78)90005-0, 1978.

Finlay, C. C., Maus, S., Beggan, C. D., Bondar, T. N., Chambodut, A., Chernova, T. A., Chulliat, A., Golovkov, V. P., Hamilton, B., Hamoudi, M., et al.: International geomagnetic reference field: the eleventh generation, Geophysical Journal International, 183, 1216–1230, https://doi.org/10.1111/j.1365-246X.2010.04804.x, 2010.

Ganiyu, S., Badmus, B., Awoyemi, M., Akinyemi, O., and Olurin, O. T.: Upward continuation and reduction to pole process on aeromagnetic data of Ibadan Area, South-Western Nigeria, Earth Science Research, 2, 66, https://doi.org/10.5539/esr.v2n1p66, 2013.

Geosoft: Gravity and magnetic modeling software user guide, 2004.

Grabarczyk, A., Wiszniewska, J., Krzemińska, E., and Petecki, Z.: A new A-type granitoid occurrence in southernmost Fennoscandia: geochemistry, age and origin of rapakivi-type quartz monzonite from the Pietkowo IG1 borehole, NE Poland, Mineralogy and Petrology, 117, 1–25, https://doi.org/10.1007/s00710-022-00799-7, 2023.

Grocott, J., Garde, A. A., Chadwick, B., Cruden, A. R., and Swager, C.: Emplacement of rapakivi granite and syenite by floor depression and roof uplift in the Palaeoproterozoic Ketilidian orogen, South Greenland, Journal of the Geological Society, 156, 15–24, https://doi.org/10.1144/gsjgs.156.1.0015, 1999.

Haapala, I. and Rämö, O. T.: Tectonic setting and origin of the Proterozoic rapakivi granites of southeastern Fennoscandia, Earth and environmental science transactions of the Royal Society of Edinburgh, 83, 165–171, https://doi.org/10.1017/S0263593300007859, 1992.

Högdahl, K., Sjöström, H., and Bergman, S.: Ductile Shear Zones Related to Crustal Shortening and Domain Boundary Evolution in the Central Fennoscandian Shield, Tectonics, 28, https://doi.org/10.1029/2008TC002277, 2009.

Ibraheem, I. M., Elawadi, E. A., and El-Qady, G. M.: Structural interpretation of aeromagnetic data for the Wadi El Natrun area, northwestern desert, Egypt, Journal of African Earth Sciences, 139, 14–25, https://doi.org/10.1016/j.jafrearsci.2017.11.036, 2018.

Jacobsen, B. H.: A Case for Upward Continuation as a Standard Separation Filter for Potential-Field Maps, Geophysics, 52, 1138–1148, https://doi.org/https://10.1190/1.1442366, 1987.

Johansson, Å., Waight, T., Andersen, T., and Simonsen, S. L.: Geochemistry and petrogenesis of Mesoproterozoic A-type granitoids from the Danish island of Bornholm, southern Fennoscandia, Lithos, 244, 94–108, https://doi.org/10.1016/j.lithos.2015.11.031, 2016.

Johansson, : A Tentative Model for the Origin of A-Type Granitoids, Minerals, 13, 236, https://doi.org/10.3390/min13020236, 2023.

Jürgenson, H.: Geoid computations in Estonia, IGeS Bulletin, 11, 21–29, 2001.

Jürgenson, H.: Eesti täppisgeoidi arvutus [Determination of Estonian precision geoid], Ph.D. thesis, Estonian University of Life Sciences, Tartu, Estonia, 157 pp. [in Estonian], 2003.

Karell, F., Ehlers, C., and Airo, M.-L.: Emplacement and magnetic fabrics of rapakivi granite intrusions within Wiborg and Åland rapakivi granite batholiths in Finland, Tectonophysics, 614, 31–43, https://doi.org/10.1016/j.tecto.2013.12.006, 2014.

https://doi.org/10.5194/egusphere-2026-6609
Preprint. Discussion started: 4 November 2026
© Author(s) 2026. CC BY 4.0 License.

Kirs, J., Huhma, H., and Haapala, I.: Petrological-chemical features and age of Estonian anorogenic potassium granites, in: Symposium on Rapakivi Granites and Related Rocks, Abstract Volume, vol. 34, pp. 28–29, Geol. Surv. Finland, 1991.

Kirs, J., Haapala, I., and Rämö, O. T.: Anorogenic magmatic rocks in the Estonian crystalline basement, in: Proceedings of the Estonian Academy of Sciences. Geology, vol. 53, pp. 210–225, https://doi.org/10.3176/geol.2004.3.05, 2004.

Kirs, J., Puura, V., Soesoo, A., Klein, V., Konsa, M., Koppelmaa, H., Niin, M., and Urtson, K.: The crystalline basement of Estonia: rock complexes of the Palaeoproterozoic Orosirian and Statherian and Mesoproterozoic Calymmian periods, and regional correlations., Estonian Journal of Earth Sciences, 58, https://doi.org/10.3176/earth.2009.4.01, 2009.

Kivisilla, J., Niin, M., and Koppelmaa, H.: Catalogue of chemical analyses of major elements in the rocks of the crystalline basement of Estonia, Geological Survey of Estonia, Tallinn, https://kirjandus.geoloogia.info/reference/21247, 1999.

Klein, V., Konsa, M., and Niin, M.: On mineralogy of the porphyrous potassium granites of small massifs in the northern Estonian basement, Proceedings of the Estonian Academy of Sciences, Geology, 43, 165–176, https://doi.org/10.3176/geol.1994.4.01, 1994.

Korhonen, J. V., Aaro, S. F., All, T., Nevanlinna, H., Skilbrei, J. R., Säävuori, H., Vaher, R., Zhdanova, L., and Koistinen, T.: Magnetic Anomaly Map of the Fennoscandian Shield 1:2,000,000, 2002.

Korja, A. and Heikkinen, P.: Proterozoic extensional tectonics of the central Fennoscandian Shield: Results from the Baltic and Bothnian Echoes from the Lithosphere experiment, Tectonics, 14, 504–517, https://doi.org/10.1029/94TC02905, 1995.

Korja, A., Korja, T., Luosto, U., and Heikkinen, P.: Seismic and geoelectric evidence for collisional and extensional events in the Fennoscandian Shield implications for Precambrian crustal evolution, Tectonophysics, 219, 129–152, https://doi.org/10.1016/0040-1951(93)90292-R, 1993.

Kosunen, P.: The rapakivi granite plutons of Bodom and Obbnäs, southern Finland: petrography and geochemistry, Bulletin of the Geological Society of Finland, 71, 275–304, https://doi.org/10.17741/bgsf/71.2.005, 1999.

Kukkonen, I. and Lauri, L. S.: Modelling the Thermal Evolution of a Collisional Precambrian Orogen: High Heat Production Migmatitic Granites of Southern Finland, Precambrian Research, 168, 233–246, https://doi.org/10.1016/j.precamres.2008.10.004, 2009.

Lahtinen, R. and Kurhila, M.: Far-field tectonic influence on the Paleoproterozoic A-type Puula granite in Fennoscandia: Implications for Svecofennian orogeny, crustal growth, and continental stabilization, Precambrian Research, 444, 108 183, https://doi.org/10.1016/j.precamres.2026.108183, 2026.

Lahtinen, R., Korja, A., and Nironen, M.: Paleoproterozoic tectonic evolution, in: Developments in Precambrian Geology, vol. 14, pp. 481–531, Elsevier, https://doi.org/10.1016/S0166-2635(05)80012-X, 2005.

Laitakari, I., Rämö, T., Suominen, V., Niin, M., Stepanov, K., and Amantov, A.: Subjotnian: Rapakivi granites and related rocks in the surroundings of the Gulf of Finland, Special Paper GTK, pp. 59–98, 1996.

Larin, A. M.: Rapakivi Granites in the Geological History of the Earth. Part 1: Magmatic Associations with Rapakivi Granites: Age, Geochemistry, and Tectonic Setting, Stratigraphy and Geological Correlation, 17, 235–258, https://doi.org/10.1134/S0869593809030010, 2009.

Loiselle, M. and Wones, D.: Characteristics and origin of anorogenic granites, Geological Society of America Abstracts with Programs, 11, 468, 1979.

Lowrie, W. and Fichtner, A.: Fundamentals of geophysics, Cambridge university press, 2020.

Maasik, V.: Gravitatsionnoe pole na territorii Éstonskoj SSR i ego primenenie: Opredelenie sily tjazhesti i poluchennye rezultaty [Gravitational field in the territory of the Estonian SSR and its application: Determination of gravity and the received results], Part 1, Institut Geologii AN ESSR, Tallinn, 156 pp. [in Russian], 1959.

https://doi.org/10.5194/egusphere-2026-6609
Preprint. Discussion started: 4 November 2026
© Author(s) 2026. CC BY 4.0 License.

Mickus, K. L., Aiken, C. L., and Kennedy, W.: Regional-residual gravity anomaly separation using the minimum-curvature technique, Geophysics, 56, 279–283, https://doi.org/10.1190/1.1443041, 1991.

Miller, C. A., Williams-Jones, G., Fournier, D., and Witter, J.: 3D gravity inversion and thermodynamic modelling reveal properties of shallow silicic magma reservoir beneath Laguna del Maule, Chile, Earth and Planetary Science Letters, 459, 14–27, https://doi.org/10.1016/j.epsl.2016.11.007, 2017.

Mitchell, M. A., Peacock, J. R., and Burgess, S. D.: Imaging the magmatic plumbing of the Clear Lake Volcanic Field using 3-D gravity inversions, Journal of Volcanology and Geothermal Research, 435, 107 758, https://doi.org/10.1016/j.jvolgeores.2023.107758, 2023.

Ndikum, E. N. and Tabod, C. T.: Applying Source Parameter Imaging (SPI) to Aeromagnetic Data to Estimate Depth to Magnetic Sources in the Mamfe Sedimentary Basin, International Journal of Geosciences, 15, 1–11, https://doi.org/10.4236/ijg.2024.151001, 2024.

Nironen, M.: The Svecofennian Orogen: A Tectonic Model, Precambrian Research, 86, 21–44, https://doi.org/10.1016/S0301-9268(97)00039-9, 1997.

Nordbäck, N., Skyttä, P., Engström, J., Ovaskainen, N., Mattila, J., and Aaltonen, I.: Mesoproterozoic Strike-Slip Faulting within the Åland Rapakivi Batholith, Southwestern Finland, Tektonika, 2, 1–26, https://doi.org/10.55575/tektonika2024.2.1.51, 2024.

Oja, T., Ellmann, A., and Märdla, S.: Gravity anomaly field over Estonia, estonian Journal of earth sciences, 68, 55–75, https://doi.org/10.3176/earth.2019.06, 2019.

Oja, T., Mäkinen, J., Bilker-Koivula, M., and Timmen, L.: Absolute gravity observations in Estonia from 1995 to 2017, Journal of Geodesy, 95, 131, https://doi.org/10.1007/s00190-021-01580-y, 2021.

Okpoli, C. and Akingboye, A.: Application of high-resolution gravity data for litho-structural and depth characterisation around Igabi area, Northwestern Nigeria, NRIAG Journal of Astronomy and Geophysics, 8, 231–241, https://doi.org/10.1080/20909977.2019.1689629, 2019.

Omietimi, E. J., Chouhan, A. K., Lenhardt, N., Yang, R., and Bumby, A. J.: Structural interpretation of the south-western flank of the Anambra Basin (Nigeria) using satellite-derived WGM 2012 gravity data, Journal of African Earth Sciences, 182, 104 290, https://doi.org/10.1016/j.jafrearsci.2021.104290, 2021.

Osagie, A. U., Eshanibli, A., and Adepelumi, A. A.: Structural trends and basement depths across Nigeria from analysis of aeromagnetic data, Journal of African Earth Sciences, 178, 104 184, https://doi.org/10.1016/j.jafrearsci.2021.104184, 2021.

Phillips, J. D.: Designing matched bandpass and azimuthal filters for the separation of potential-field anomalies by source region and source type, ASEG Extended Abstracts, 2001, 1–4, https://doi.org/10.1071/ASEG2001ab110, 2001.

Pirajno, F. and Santosh, M.: Mantle plumes, supercontinents, intracontinental rifting and mineral systems, Precambrian Research, 259, 114–142, https://doi.org/10.1016/j.precamres.2014.12.016, 2015.

Potagin, C.: Geology, Geochemistry, and Geochronology of the Märjamaa Rapakivi Granitoid Intrusion, Master's thesis, Tallinn University of Technology, Tallinn, Estonia, https://digikogu.taltech.ee/et/Download/9ee436a4-89a6-487b-8d09-c957cb76666e, master's thesis, Department of Geology, Institute of Geology. Supervisors: Alvar Soesoo and Juan David Solano-Acosta, 2024.

Pratt, D. A. and Shi, Z.: An improved pseudo-gravity magnetic transform technique for investigation of deep magnetic source rocks, ASEG Extended Abstracts, 2004, 1–4, https://doi.org/10.1071/ASEG2004ab116, 2004.

Puura, V. and Flodén, T.: Subjotnian igneous structures in the Svecofennian domain of the Baltic region, GFF, 118, 22–23, https://doi.org/10.1080/11035899609546289, 1996.

Puura, V. and Flodén, T.: Rapakivi-granite–anorthosite magmatism — a way of thinning and stabilisation of the Svecofennian crust, Baltic Sea Basin, Tectonophysics, 305, 75–92, https://doi.org/10.1016/S0040-1951(99)00019-0, 1999.

https://doi.org/10.5194/egusphere-2026-6609
Preprint. Discussion started: 4 November 2026
© Author(s) 2026. CC BY 4.0 License.

Puura, V. and Flodén, T.: Rapakivi-related basement structures in the Baltic Sea area; a regional approach, GFF, 122, 257–272, https://doi.org/10.1080/11035890001223257, 2000.

Raukas, A. and Teedumäe, A., eds.: Geology and Mineral Resources of Estonia, Estonian Academy Publishers, Tallinn, Estonia, https://geoloogia.info/geology/index.html, ISBN 9985-50-185-3, 1997.

Rämö, O. T. and Haapala, I.: One hundred years of rapakivi granite, Mineralogy and Petrology, 52, 129–185, https://doi.org/10.1007/BF01163243, 1995.

Rämö, O. T. and Haapala, I.: Rapakivi granites, Developments in Precambrian Geology, 14, 533–562, https://doi.org/10.1016/S0166-2635(05)80013-1, 2005.

Rämö, O. T., Huhma, H., and Kirs, J.: Radiogenic isotopes of the Estonian and Latvian rapakivi granite suites: new data from the concealed Precambrian of the East European Craton, Precambrian Research, 79, 209–226, https://doi.org/10.1016/S0301-9268(95)00083-6, 1996.

Saada, S. A., Mickus, K., Eldosouky, A. M., and Ibrahim, A.: Insights on the tectonic styles of the Red Sea rift using gravity and magnetic data, Marine and Petroleum Geology, 133, 105–253, https://doi.org/10.1016/j.marpetgeo.2021.105253, 2021.

Saibi, H., Nishijima, J., Ehara, S., and Aboud, E.: Integrated gradient interpretation techniques for 2D and 3D gravity data interpretation, Earth, planets and space, 58, 815–821, https://doi.org/10.1186/BF03351986, 2006.

Salminen, J., Elming, S.-Å., Mertanen, S., Wang, C., Almqvist, B., and Moakhar, M. O.: Paleomagnetic studies of rapakivi complexes in the Fennoscandian shield–Implications to the origin of Proterozoic massif-type anorthosite magmatism, Precambrian Research, 365, https://doi.org/10.1016/j.precamres.2021.106406, 2021.

Selonen, O., Ehlers, C., Luodes, H., and Lerssi, J.: The Vehmaa rapakivi granite batholith - An assemblage of successive intrusions indicating a piston-type collapsing centre, Bulletin of the Geological Society of Finland, 77, https://doi.org/10.17741/bgsf/77.1.004, 2005.

Senger, K., Ammerlaan, F., Betlem, P., Brönner, M., Dumais, M.-A., Gellein, J., Henningsen, T., Janocha, J., Johannessen, E. P., Liebsch, J., Solano-Acosta, J. D., et al.: Crustal heterogeneity onshore central Spitsbergen: Insights from new gravity and vintage geophysical data, Geochemistry, Geophysics, Geosystems, 26, https://doi.org/10.1029/2024GC011563, 2025.

Sharkov, E.: Middle-proterozoic anorthosite–rapakivi granite complexes: An example of within-plate magmatism in abnormally thick crust: Evidence from the East European Craton, Precambrian Research, 183, 689–700, https://doi.org/10.1016/j.precamres.2010.08.008, 2010.

Siachoque, A., Salazar, C. A., and Trindade, R.: Emplacement and deformation of the A-type Madeira granite (Amazonian Craton, Brazil), Lithos, 277, 284–301, https://doi.org/10.1016/j.lithos.2016.10.021, 2017.

Skridlaitė, G., Whitehouse, M., and Rimša, A.: Evidence for a pulse of 1.45 Ga anorthosite–mangerite–charnockite–granite (AMCG) plutonism in Lithuania: implications for the Mesoproterozoic evolution of the East European Craton, Terra Nova, 19, 294–301, https://doi.org/10.1111/j.1365-3121.2007.00748.x, 2007.

Soesoo, A.: Estonian porphyraceous potassium granites: petrochemical subdivision and petrogenetical interpretation, in: Proceedings of the Estonian Academy of Sciences, Geology, vol. 42, pp. 97–109, https://doi.org/10.3176/geol.1993.3.01, 1993.

Soesoo, A. and Hade, S.: Geochemistry and age of some A-type granitoid rocks of Estonia, in: Seventh symposium on the structure, composition and evolution of the lithosphere in Finland, p. 97, 2012.

Soesoo, A. and Niin, M.: Petrographical and petrochemical features of the Estonian Precambrian porphyraceous potassium granites, in: Proceedings of the Estonian Academy of Science, Geology, vol. 41, pp. 93–107, https://doi.org/10.3176/geol.1992.3.01, 1992.

Soesoo, A., Puura, V., Kirs, J., Petersell, V., Niin, M., and All, T.: Outlines of the Precambrian basement of Estonia, in: Proceedings of the Estonian Academy of Sciences, Geology, vol. 53, pp. 149–164, https://doi.org/10.3176/geol.2004.3.02, 2004.

https://doi.org/10.5194/egusphere-2026-6609
Preprint. Discussion started: 4 November 2026
© Author(s) 2026. CC BY 4.0 License.

Soesoo, A., Nirgi, S., and Plado, J.: The evolution of the Estonian Precambrian basement: geological, geophysical and geochronological constraints, Proceedings of the Karelian Research Centre of the Russian Academy of Sciences, pp. 18–33, https://doi.org/10.17076/geo1185, 2020.

Solano Acosta, J. D.: Crustal Structure, Tectonics, and Magmatic Evolution of the Estonian Proterozoic Basement: Geophysical and Geochemical Insights, Ph.D. thesis, Tallinn University of Technology, ISBN 978-9916-80-450-6, https://doi.org/10.23658/taltech.9/2026, 2026.

Solano-Acosta, J. D.: Major-Element Geochemistry, Redox Systematics, and Petrogenesis of the Estonian Rapakivi Intrusions, Finnish Wiborg Batholith, and Onas intrusion: A Revised Analysis of Fennoscandian AMCG Magmatism, EGUsphere, https://doi.org/10.5194/egusphere-2026-4451, [preprint], 2026.

Solano-Acosta, J. D., Soesoo, A., and Hints, R.: New insights of the crustal structure across Estonia using satellite potential fields derived from WGM-2012 gravity data and EMAG2v3 magnetic data, Tectonophysics, 846, 229 656, https://doi.org/10.1016/j.tecto.2022.229656, 2023.

Solano-Acosta, J. D., Soesoo, A., and Hints, R.: Integrated geophysical and emplacement modelling of the Märjamaa and Kloostri rapakivi granitoids, Estonia: Insights into intrusion geometry and tectonic controls, Precambrian Research, 430, 107 938, https://doi.org/10.1016/j.precamres.2025.107938, 2025a.

Solano-Acosta, J. D., Soesoo, A., and Hints, R.: Geochemistry, provenance, and tectonic setting of Paleoproterozoic metasedimentary and metavolcanic units of the Estonian Alutaguse region, eastern Fennoscandia, Estonian Journal of Earth Sciences, 74, 61–82, https://doi.org/10.3176/earth.2025.05, 2025b.

Solano-Acosta, J. D., Graul, S., Soesoo, A., Hints, R., Vind, J., and Liivamägi, S.: Exploration of critical elements in the concealed North Estonian basement and its Eastern Fennoscandian context, European Geologist, https://doi.org/10.5281/zenodo.18978768, 2026a.

Solano-Acosta, J. D., Pearse, J., and Despaigne-Diaz, A. I.: Morphotectonic Analysis of Upper Guajira Region, Colombia Using Multi-Resolution DEMs, Landsat-8, and WGM-12 Data, Geosciences, 16, 52, https://doi.org/10.3390/geosciences16010052, 2026b.

Solano-Acosta, J. D., Soesoo, A., and Hints, R.: An Updated Review of Major-Element Geochemistry, Redox Systematics, and Petrogenesis of the Märjamaa and Kloostri Rapakivi Granites, Estonia, Estonian Journal of Earth Sciences, https://doi.org/10.3176/earth.2026.06, 2026c.

Soosalu, H., Uski, M., Komminaho, K., and Veski, A.: Recent Intraplate Seismicity in Estonia, East European Platform, Seismological Research Letters, 93, 1800–1811, https://doi.org/10.1785/0220210277, 2022.

Suominen, V.: The chronostratigraphy of southwestern Finland with special reference to Postjotnian and Subjotnian diabases, Bulletin-Geological Survey of Finland, 1991.

Valkama, M., Sundblad, K., Nygård, R., and Cook, N.: Mineralogy and geochemistry of indium-bearing polymetallic veins in the Sarvlaxviken area, Lovisa, Finland, Ore Geology Reviews, 75, 206–219, https://doi.org/10.1016/j.oregeorev.2015.12.001, 2016.

Vigneresse, J. L.: The specific case of the Mid-Proterozoic rapakivi granites and associated suite within the context of the Columbia supercontinent, Precambrian research, 137, 1–34, https://doi.org/10.1016/j.precamres.2005.01.001, 2005.